Organic Aerosol Formation from Photochemical Oxidation of Diesel Exhaust in a Smog Chamber

ARTICLE *in* ENVIRONMENTAL SCIENCE AND TECHNOLOGY · NOVEMBER 2007

Impact Factor: 5.33 · DOI: 10.1021/es070193r · Source: PubMed

5 AUTHORS, INCLUDING:

J. R. Pierce
Colorado State University
111 PUBLICATIONS **2,183** CITATIONS
SEE PROFILE

Neil M Donahue
Carnegie Mellon University
270 PUBLICATIONS **10,572** CITATIONS
SEE PROFILE

Organic Aerosol Formation from Photochemical Oxidation of Diesel Exhaust in a Smog Chamber

EMILY A. WEITKAMP, AMY M. SAGE, JEFFREY R. PIERCE, NEIL M. DONAHUE, AND ALLEN L. ROBINSON*

Center for Atmospheric Particle Studies, Carnegie Mellon University, 5000 Forbes Avenue, Pittsburgh, Pennsylvania 15213

Diluted exhaust from a diesel engine was photo-oxidized in a smog chamber to investigate secondary organic aerosol (SOA) production. Photochemical aging rapidly produces significant SOA, almost doubling the organic aerosol contribution of primary emissions after several hours of processing at atmospherically relevant hydroxyl radical concentrations. Less than 10% of the SOA mass can be explained using a SOA model and the measured oxidation of known precursors such as light aromatics. However, the ultimate yield of SOA is uncertain because it is sensitive to treatment of particle and vapor losses to the chamber walls. Mass spectra from an aerosol mass spectrometer (AMS) reveal that the organic aerosol becomes progressively more oxidized throughout the experiments, consistent with sustained, multi-generational production. The data provide strong evidence that the oxidation of a wide array of precursors that are currently not accounted for in existing models contributes to ambient SOA formation.

Introduction

Organic material contributes a significant fraction of ambient fine-particle mass (*1*, *2*). Organic aerosol (OA) is directly emitted to the atmosphere (primary OA); it is also generated in the atmosphere from low-volatility products of gas-phase reactions (secondary organic aerosol or SOA). The design of effective regulations requires an understanding of the relative contribution of these two fractions; however, the primary−secondary split is uncertain. Past research suggests that primary OA is dominant in urban areas, except during photochemical episodes (*3*−*5*). On a global scale, SOA is thought to contribute more than half of the total OA burden (*1*).

Recent field measurements suggest that SOA contributes the dominant fraction of the OA even in urban environments (*6*, *7*). This SOA cannot be explained by current models and has been attributed to some unaccounted for component of the anthropogenic emissions (*6*, *8*). The dominant anthropogenic SOA precursors are thought to be light aromatics such as toluene, *m*-/*p*-/*o*-xylenes, and ethylbenzene (*5*, *9*, *10*). Odum et al. (*11*, *12*) found that the oxidation of aromatic precursors could account for the majority of SOA formed from photo-oxidation of whole gasoline vapors in a smog chamber. While fuel vapors are present in vehicle emissions, they may not accurately represent the true SOA-forming potential of actual emissions because aromatics and other known SOA precursors typically contribute a small fraction of the total organic emissions (*13*, *14*).

In this paper, we report results from the photo-oxidation of diluted exhaust from a diesel engine in a smog chamber. We measured the evolution of the gas and particle phases to determine the total SOA production. We then compared the measured production with the predictions of an SOA model and will discuss the implications of the results.

Materials and Methods

Experimental Setup. Experiments were conducted in the Carnegie Mellon University smog chamber, which is a light- and temperature-controlled room that houses a 10 m^3 Teflon bag. Before each experiment, the chamber was cleaned by irradiation, heat (40 °C), and continuous flushing with dry, HEPA-filtered and activated carbon-filtered air for several hours. After cleaning, the lights were turned off, and the chamber temperature was reduced to 23 ± 1 °C with an initial relative humidity of ∼5%. A small amount of exhaust was then added through a heated inlet from a single-cylinder diesel engine (Yanmar L70AE) connected to a 4.5 kW generator. After allowing time for mixing, the exhaust was photo-oxidized by exposure to UV light produced by an array of 88 black lights (64 GE F40BL UVA and 24 GE F20BL UVA). Photo-oxidation refers to the light-initiated chemistry that includes the formation of oxidants such as ozone and the hydroxyl radical ($OH^{\bullet}$). Experiments were conducted at several initial exhaust concentrations and with the engine operated at idle, low (30% of rated capacity), and medium load (60% of rated capacity). Control experiments were conducted to verify that there was no new particle formation in a cleaned bag exposed to the black lights or in a non-illuminated chamber containing diluted diesel exhaust. The engine was operated for at least 20 min to prior to sample introduction, and the diesel fuel was purchased at a local gas station.

Gas and particle concentrations were continuously monitored during the 3−9 h experiments. The particle size and number were measured using a scanning mobility particle sizer (SMPS, TSI 3080) equipped with a long differential mobility analyzer electrode (TSI 3081). The particle mass was estimated assuming spherical particles and a density of 1 g cm^{-3}. Continuous in situ measurements of the average particle chemical composition were made using a quadrupole aerosol mass spectrometer (Q-AMS, Aerodyne Research Inc.), which was operated in alternating mode (*15*).

Concentrations of organic gas-phase constituents were measured using a proton-transfer reaction mass spectrometer (PTR-MS, Ionicon Analytik) operated in selective-ion mode. Masses monitored included $m/z = 79$, 93, 107, 121, and 129, which correspond to benzene, toluene, the three xylene isomers (*m*-/*p*-/*o*-xylene), ethylbenzene, trimethylbenzenes, and naphthalene, respectively. These masses are not unique to these species; for example, the three xylenes, ethylbenzene, benzaldehyde, and perhaps additional species all appear at mass 107 (*16*). Here, we attribute the entire PTR-MS signal at m/z 93 and 107 to toluene and xylenes, respectively. This assumption may overestimate the concentrations of these SOA precursors, thus maximizing our estimates of their potential SOA production. The PTR-MS was calibrated using a standard from Spectra Gases.

Average OH concentrations were calculated from the measured decay of toluene and its rate constant for reaction with OH ($k_{OH} = 5.7 \times 10^{-12}$ cm^3 $molecules^{-1}$ s^{-1}) (*17*). Typical

* Corresponding author phone: (412)268-3657; fax: (412)268-3348; e-mail: alr@andrew.cmu.edu.

OH levels were 3 (±1) × 10^6 molecules cm^{-3}, representative of daytime concentrations in the summer. NO_x concentrations were not measured in the chamber but were assumed to be high (i.e., high-NO_x conditions) based on typical NO_x emission factors for diesel engines (*18*).

Quantifying SOA Production. To determine the total SOA production, we must account for the loss of both particle mass and condensable vapors to the chamber walls. We formulate the problem in terms of the particle mass balance. The change in the suspended particle mass in the chamber, C_{sus}, is

$$\frac{d}{dt}[C_{sus}] = -k_w C_{sus} + \dot{P}_{sus} \quad (1)$$

where $k_w C_{sus}$ is the loss rate of particle mass to the chamber walls and $\dot{P}_{sus}$ is the production rate of the new particle mass or SOA on the suspended particles. Similarly, the change in particle mass on the walls, C_{wall}, is

$$\frac{d}{dt}[C_{wall}] = +k_w C_{sus} + \dot{P}_{wall} \quad (2)$$

where $\dot{P}_{wall}$ is the loss rate of condensable vapors (SOA) to the walls. The goal is to determine the total production rate of new particle mass: $\dot{P}_{wall} + \dot{P}_{sus}$.

$\dot{P}_{sus}$ is determined by numerically evaluating eq 1 using the time-series of the measured C_{sus} (determined from the SMPS measurements) and an estimate of k_w (the first order total mass wall-loss rate). k_w is an uncertain parameter that depends on the details of the particle size and charge distribution and the level of turbulence inside the chamber. We have used several approaches to estimate k_w to illustrate the uncertainty in the estimated SOA production associated with different wall-loss treatments. The primary estimates are based on an algorithm that solves the discrete general dynamics equation (*19*). Briefly, a measured size distribution is used as the initial condition for the general dynamics equation, which is then integrated forward in time explicitly accounting for coagulation and using estimates for the wall-loss and condensation/evaporation rates. The predicted size distribution is compared to the actual size distribution measured during the subsequent SMPS scan (SMPS scans are typically 3 min apart). The estimates of k_w and the condensation/evaporation rates are then updated, and the process is repeated until the predicted and measured size distributions match. This procedure is applied for each pair of SMPS scans to estimate k_w as function of time. The algorithm requires making an assumption regarding the size dependence of wall-loss. In this paper, we consider two cases. In the first case, for a given SMPS scan, we assumed that the wall-loss is not size dependent. This assumption is strictly valid for a monodisperse aerosol but becomes progressively less accurate as the size distribution becomes wider. The second case accounts for the size dependence of the wall-loss using an empirical expression based on turbulent deposition and particle charge. Both of these cases perform acceptably (relative errors of less than 25%) on control experiments using ammonium sulfate and biogenic SOA. Additional details of this algorithm and its performance are described in an upcoming publication (*19*).

We also estimated k_w by fitting the measured decay of particle mass inside the chamber when the black lights are off. As expected, this approach shows that k_w decreases with time as the particle size distribution grows. This evolution was accounted for by linear interpolating the wall-loss rate either with time or with the median particle diameter.

To determine $\dot{P}_{wall}$, we assume that the fraction of SOA that forms on the suspended mass is related to the ratio of the particle mass on the walls to that in suspension

$$\dot{P}_{wall} = \dot{P}_{sus}\left(\frac{\omega C_{wall}}{C_{sus}}\right) \quad (3)$$

where ω is a proportionality factor. When the condensable products only partition to the suspended particles, $\omega = 0$ and $\dot{P}_{wall} = 0$. When the material lost to the walls remains completely in equilibrium with the gas phase, $\omega = 1$. We consider both of these limiting cases. One conclusion we can draw immediately is that the uncertainty from condensation/evaporation to the walls ($\dot{P}_{wall}$) scales with the particle mass fraction on the walls: the more particle mass on the walls, the larger the uncertainty in the total mass for any experiment with either ongoing chemistry or changing temperature.

SOA Contribution from Known Gas-Phase Precursors. We use the SOA model SOAM II to quantify the new particle mass formed from the oxidation products of known gas-phase SOA precursors (*9*). Our analysis considers 58 SOA precursors, including aromatics, alkanes, and alkenes. The oxidation rate of each precursor was determined from the PTR-MS data. For each SOA precursor, SOAM II defines yields and partitioning coefficients of a set of lumped condensable products (*9*). These parameters were determined by fitting laboratory smog chamber data using absorption partitioning theory following the approach of Odum et al. (*12*). We have implemented SOAM II in a box model that tracks the concentration and partitioning of condensable products inside the smog chamber. The model accounts for the loss of condensable products to the chamber walls, using a framework similar to that described in the previous section. The partitioning of the condensable products is calculated using an absorptive partitioning theory, assuming that each product forms an ideal solution with the entire aerosol mass measured using the SMPS. Additional details on the SOA model are provided in the Supporting Information.

Concentrations of nine of the 58 precursor species are directly measured by PTR-MS and account for over 90% of the SOA mass predicted by the model. These are benzene, toluene, *m*-/*p*-/*o*-xylenes, ethylbenzene, 1,2,4-trimethylbenzene, 1,3,5-trimethylbenzene, and naphthalene. The precursors that were not directly measured include *n*-alkanes, branched alkanes, cycloalkanes, aromatic aldehydes, and unsaturated compounds. We estimated the initial concentrations of these unmeasured species by combining the measured initial toluene concentration with the emission ratios specified in Schauer et al. (*14*). The emissions of aromatics from our engine agree well with the Schauer et al. (*14*) diesel profile. For example, the ratio of toluene to organic carbon mass is 0.09 in Schauer et al. (*14*), while the measured ratio for a typical experiment in this study was 0.14. As stated previously, the estimated decay of the unmeasured precursors contributed less than 10% of the total SOA mass predicted by SOAM II, so differences between our generator emissions and the medium-duty diesel emissions used in Schauer et al. (*14*) should not significantly affect the predicted SOA mass.

Results

Time-series measurements from a typical experiment are shown in Figure 1. The initial aerosol mass was 58 $\mu g\ m^{-3}$, all of which is primary diesel particulate matter. At time zero, the black lights were turned on to initiate photochemistry, resulting in a rapid and substantial production of new particle mass. For the first hour, Figure 1a shows that the suspended mass actually increases, indicating that the production rate is greater than the wall-loss rate. After about an hour, the

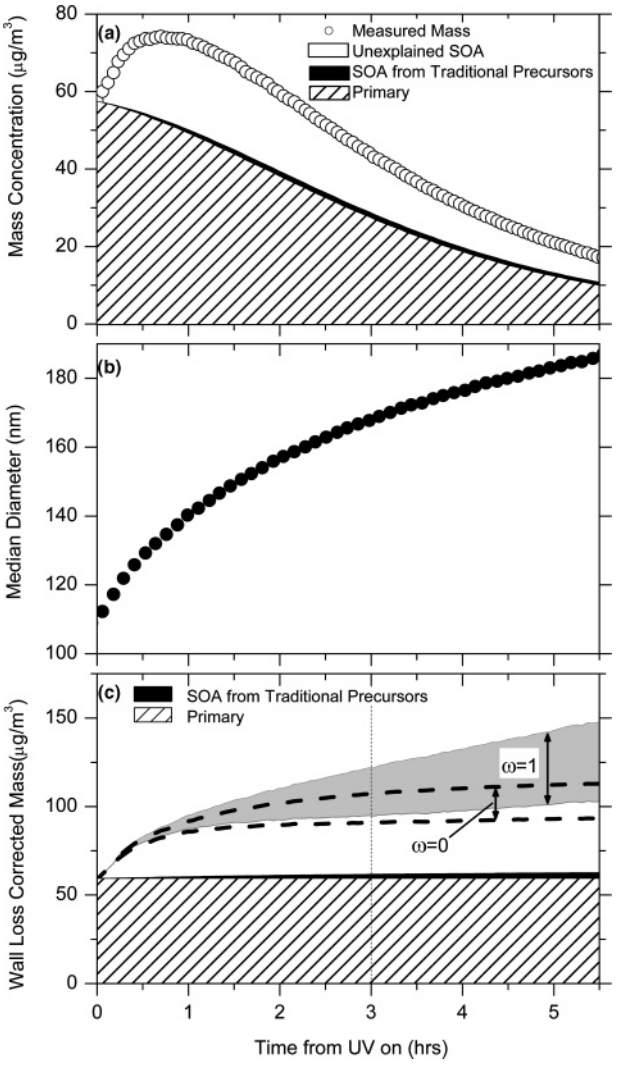

FIGURE 1. Time-series of (a) measured suspended mass, (b) mass−median diameter, and (c) wall-loss corrected mass measured during photo-oxidation of diesel exhaust. Striped region indicates total primary particulate mass based on the initial mass and the estimated wall-loss rate. The dashed lines in panel c represent the range of wall-loss corrected mass assuming no loss of condensable vapors to the walls: $\omega = 0$ in eq 3. The gray area indicates the range of wall-loss corrected mass assuming that the aerosols lost to the walls remain in equilibrium with the suspended vapors: $\omega = 1$ in eq 3. Vertical solid line indicates $t = 3$ h and corresponds to Figure 3.

production rate slows, and the suspended mass decreases due to wall-losses. Figure 1b shows that the median particle diameter increases throughout the experiment, consistent with condensational growth.

Before quantifying the production of secondary aerosol mass, we examine its composition using the AMS data. AMS measures the size and composition of the non-refractory portion of the suspended aerosol, including organics, sulfate, and nitrate (*15*). It does not measure elemental carbon (EC).

The AMS data indicate that the secondary aerosol formed in the chamber is organic. More than 80% of the non-refractory suspended aerosol mass is organic throughout every experiment. Diesel fuel does contain sulfur, and diesel engines emit NO_x. The AMS data indicate that sulfate and nitrate contribute at most 11 and 6%, respectively, of the non-refractory aerosol mass. Furthermore, there is no evidence of sulfate or nitrate aerosol production during photo-oxidation. The lack of secondary nitrate and sulfate

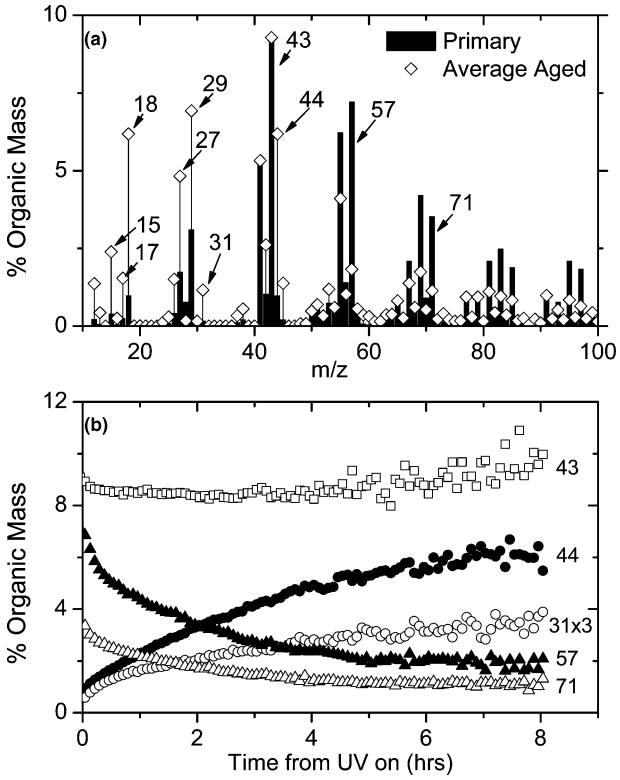

FIGURE 2. Mass spectra measured using an aerosol mass spectrometer. (a) Average percent organic mass measured at different *m/z* at the beginning (primary) and end (aged) of an experiment. (b) Time-series of key masses: *m/z* 57 and 71 are indicators of primary or fresh emissions, *m/z* 44 and 31 are indicators of oxidation and aging, and *m/z* 43 indicated both fresh and aged OA. In panel b, the signal for *m/z* 31 has been multiplied by a factor of 3.

is not surprising. The rate constant for SO_2 + OH is about an order of magnitude slower than that of large saturated organics with OH (*20*, *21*). Nitrate only condenses into the particle phase when there is free ammonia (or another cation) available to neutralize it (*22*).

The composition of the organics evolves during photo-oxidation. Figure 2a presents the AMS mass spectrum of the total organic mass measured at the beginning and end of the experiment shown in Figure 4. The spectrum of the fresh emissions looks like diesel exhaust measured in vehicle chase studies (*32*). It has a strong $C_nH_{2n+1}^+$ sequence (*m*/*z* 29, 43, 57, 71, 85...) that is characteristic of alkanes and a prominent $C_nH_{2n-3}^+$ sequence (*m*/*z* 67, 81, 95, 107...) that is associated with cycloalkanes (*27*, *32*, *34*). The aged OA mass spectrum shown in Figure 2a is averaged over the last hour of the experiment. Relative to the fresh emissions, the signal in the aged mass spectrum is shifted toward smaller fragments, indicating the presence of more highly functionalized species.

A time-series of several key AMS mass fragments is plotted in Figure 2b. The data show that the organic aerosol becomes progressively more oxidized throughout the experiment. Mass fragments such as *m*/*z* 57 ($C_4H_9^+$) and 71 ($C_5H_{11}^+$) that are associated with fresh emissions decrease, while fragments such as *m*/*z* 44 (CO_2^+) and 31 (CH_3O^+) that are associated with oxidized organics increase in relative importance. Both fresh primary and oxidized OA contributed to the *m*/*z* 43 signal ($C_3H_7^+$ and $C_2H_3O^+$ fragments), which remains constant throughout the experiment. While some of the oxidation may be due to heterogeneous chemistry, the flux of hydroxyl radicals to the particles is far too small to explain the extent of the observed oxidation. Therefore, Figure 2b provides clear evidence of sustained SOA production. The AMS composition data are discussed in detail in ref *26*.

Quantifying SOA Production. In this section, we correct the data for wall-losses to quantify the SOA production. Figure 1a shows the estimated contribution of primary aerosol to the measured suspended aerosol mass based on the estimated wall-loss rate. The wall-loss corrected mass is plotted in Figure 1c. In this framework, the primary aerosol mass is constant, a potentially conservative assumption since heterogeneous oxidation may cause some of the primary mass to evaporate (*23*). SOA production may also alter the gas-particle partitioning of the primary emissions. Any SOA production increases the wall-loss corrected mass.

Assumptions regarding the wall-loss correction represent the largest uncertainty for quantifying the SOA production. To illustrate this uncertainty, several estimates of the wall-loss corrected mass are shown in Figure 1c. The two dashed lines bound the wall-loss corrected mass, assuming that no condensable vapors are lost to the walls—$\omega = 0$ in eq 3—thus, they represent SOA production only on the suspended aerosol ($\dot{P}_{sus}$). The gray area bounds the wall-loss corrected mass assuming that the aerosols lost to the walls remain in equilibrium with the suspended vapors: $\omega = 1$ in eq 3. There is no obvious reason as to why particles deposited to the chamber walls should lose contact with the vapors in the chamber, a conclusion supported by precursor spiking experiments such as the one described in the next section. Therefore, the gray region in Figure 1c represents our best estimate of the wall-loss corrected mass and the SOA yield.

There are several important conclusions to be drawn from Figure 1c. First, there is the rapid and substantial production of SOA. This conclusion is not sensitive to the wall-loss correction. Even for the lower-bound estimate, the wall-loss corrected mass has increased by 60% by the end of the experiment shown in Figure 1. The other wall-loss corrections show greater production.

Second, the ultimate yield of SOA is uncertain because it depends strongly on the wall-loss correction. Although the dashed lines in Figure 1c indicate that k_w and thus $\dot{P}_{sus}$ are reasonably well-constrained (e.g., by the end of the experiment, the upper-bound estimate is 21% higher than the lower-bound estimate), the diverging gray area illustrates the uncertainty associated with the loss of condensable vapors to the walls throughout the experiment. As more mass is lost to the walls, the SOA production rate becomes extremely sensitive to the uncertainty in k_w when $\omega = 1$.

Third, our best estimate (gray area in Figure 1c) indicates that, although the SOA production rate varies with time, there is sustained production throughout the experiment. The rapid initial production signifies a substantial pool of precursors that is rapidly consumed. The subsequent production is slower, but still significant; for example, 37% of the SOA is formed after the initial hour of UV exposure based on the lower-bound estimate of the gray area in Figure 1. OH levels in the chamber were only 3×10^6 molecules cm^{-3}, about half the peak summertime levels. Therefore, the slower, but sustained production contributes substantial SOA on atmospherically relevant timescales. At these OH levels, one generation of oxidation occurs every 3−5 h based on rate constants for typical large saturated and unsaturated species (*17*). Therefore, sustained production likely involves multiple generations of processing, meaning that the pool of precursor vapors is not exhausted but rather evolves with continuing chemistry.

The trends shown in Figure 1 were observed across multiple experiments conducted at different engine loads and initial aerosol concentrations. Figure 3 plots the estimated fraction of wall-loss corrected organic mass that is primary and secondary after 3 h of aging for all experiments. Two bars are shown for each experiment corresponding to the upper- and lower-bound estimates for SOA production (e.g., the lowest dashed line and the upper edge of the gray region in Figure 1c). Substantial SOA production was observed across all experiments.

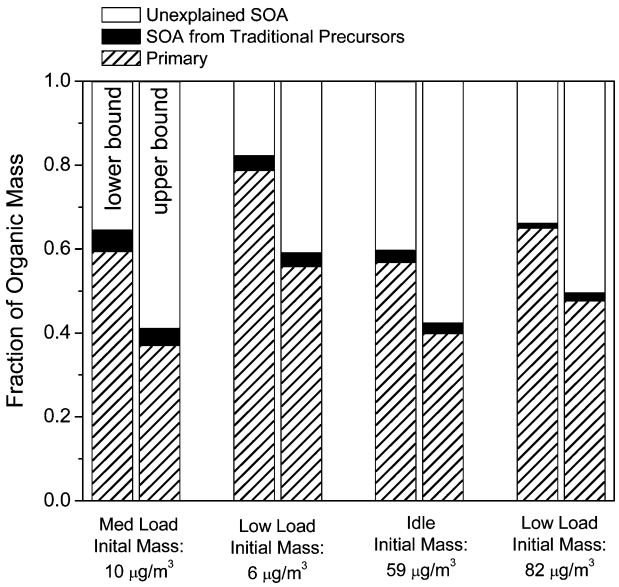

FIGURE 3. Fractional contribution of primary organic aerosol, SOA from oxidation of known precursors, and unexplained SOA to the total SOA. Both upper- and lower-bound estimates for the SOA production are shown for experiments conducted at different engine loads and initial aerosol concentrations. Initial concentrations stated in *x*-axis labels are concentrations of total primary particulate mass, not initial OA.

Figure 3 indicates that SOA contributes, at a lower bound, 20−60% to the wall-loss corrected organic aerosol concentrations after only 3 h of aging. An additional uncertainty is that the primary organic aerosol concentration was not directly measured. It was calculated based on the total aerosol mass measured by the SMPS subtracting estimates of the contribution of EC and sulfate. The EC contribution was based on previous emission tests performed with this engine at similar loads. About 20% of the $PM_{2.5}$ mass emissions is EC at low load and about 40% at medium load (*24*). We also assumed that 10% of the mass was sulfate based on the AMS data. This estimate does not account for other, non-carbonaceous components and therefore represents an upper-bound for the contribution of primary organic aerosol. Lipsky et al. (*24*) report that artifact corrected estimates of the organic mass fraction may be as little as 40% for low load and 20% for medium load (multiplying organic carbon (OC) by 1.4 to convert the data to organic mass). Using a lower-bound estimate for the primary organic mass in Figure 3 increases the relative contribution of SOA to over 50% for all experiments after only 3 h of aging.

Although the wall-loss correction is the major uncertainty in SOA production estimates, our analysis also makes assumptions about the particle density, particle sphericity, and diesel aerosol composition. These uncertainties can be constrained using the AMS data, which provide an independent estimate of the non-refractory mass. Both the AMS measured non-refractory mass (not presented) and the SMPS integrated volume (shown in Figures 1 and 3) indicate a substantial secondary aerosol production, especially in the first hour of the experiments. However, the AMS mass data also require wall-loss correction and therefore provide little additional insight into the ultimate SOA yield. Decomposition of the AMS mass spectra provides independent estimates of the amount of SOA that matches closely with the SMPS results presented here (*25*, *26*). Therefore, multiple pieces of independent evidence support the conclusion of substantial SOA production.

Detailed comparisons of the particle size distributions measured with SMPS and AMS suggest that the initial effective

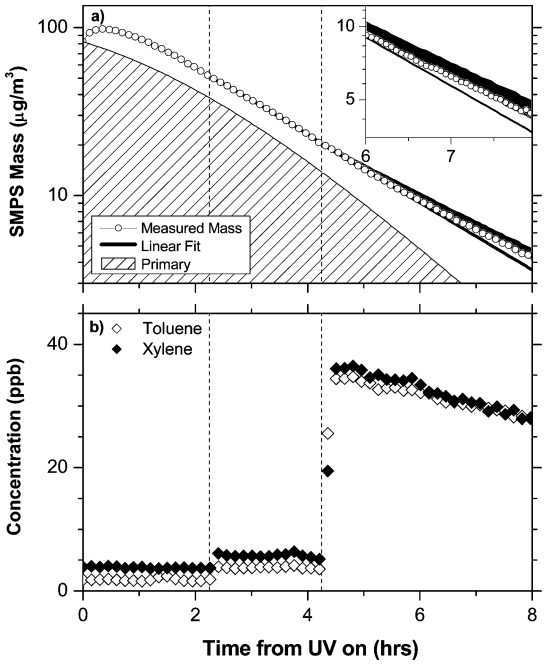

FIGURE 4. Time-series of (a) suspended aerosol mass and (b) toluene and xylene concentrations measured during photo-oxidation of diesel exhaust. The striped region is the estimated primary concentration based on the initial aerosol concentration and wall-loss rate. Vertical dashed lines show precursor spikes. Solid black line in panel a indicates a log linear fit of the data between the first and the second spikes, and the gray region in panel a represents the model estimate from known SOA precursors added to the solid black line for the $\omega = 0$ (top border) and $\omega = 1$ (bottom border) limits as discussed in the text. Inset in panel a magnifies the last 2 h of the experiment and shows that the measured mass follows the $\omega = 1$ line, indicating that the mass on the walls remains in phase equilibrium with the suspended mass.

particle density increases by 20−30% during the first half hour of an experiment when SOA is rapidly formed. This may reflect the coating of the fractal-like primary diesel particles. This increase in density (or change of shape) is not accounted for in the wall-loss model and means that we may be underestimating SOA produced in the initial stages of the experiment by 20−30%.

Contribution of Known SOA Precursors. After establishing that there is substantial SOA production, we investigated the contribution of known precursors using the previously described SOA model and the PTR-MS data and by spiking the chamber with aromatics.

The predictions of the SOA model are shown in Figure 1. By the end of the experiment, the SOA formed from oxidation products of known precursors explains less than 8% of the new particle mass for the $\omega = 0$ case and less than 7% for the $\omega = 1$ case, forming a barely visible black sliver in Figure 1c.

Figure 3 shows that the oxidation of known precursors contributed a very small fraction of SOA in all experiments. These precursors only explain between 2 and 8% of our lower estimate of the new particle mass. Their contribution is so small that even if we significantly increased the SOA yields from known precursors beyond that measured in previous smog chamber experiments, substantial amounts of unexplained SOA would remain.

We also investigated the contribution of known precursors by spiking the smog chamber with aromatics. Figure 4 shows results from an experiment in which two aliquots of toluene and *p*-xylene were added to the chamber, one at 2.2 h and a second at 4.2 h after the black lights were turned on. Figure 4a plots the measured aerosol mass on a log scale, along with an estimate of primary mass based on the wall-loss rate. As in all the experiments, when the black lights were turned on, substantial SOA was formed. Figure 3b shows toluene and xylene concentrations measured with the PTR-MS. The initial toluene and xylene concentrations were 2 ± 0.2 and 4 ± 0.4 ppbv, respectively. This first spike almost doubled the concentration of these two traditional SOA, and the second spike increased their concentrations by a factor of ∼10. The concentration of the aromatics slowly decays over the course of the experiment.

Figure 4a shows that these spikes had little effect on the measured aerosol mass. If aromatics produced a large fraction of SOA, we would expect a large kink in the suspended aerosol mass, especially for the second spike, which effectively doubled the potential SOA production from all measured aromatics. The spiking experiments provide strong evidence that light aromatics are not the dominant precursors in our experiment. A key issue is the mildly oxidizing conditions inside the chamber. Although there are sufficient aromatics to produce substantial SOA, their oxidation rates are much too slow under the conditions of these experiments. The characteristic time for toluene oxidation is about 16 h for these experiments.

The spiking experiment shown in Figure 4 also provides insight into the potential loss of condensable vapors to the chambers walls (the value of ω). As a reference point, we first calculated a log-linear fit of the measured aerosol mass between the first and the second spike to estimate how the suspended aerosol mass would have changed if there were no second spike. Comparing this line to the measured mass reveals that the second spike modestly increased the SOA production rate. We then used the SOA model to calculate the aerosol mass produced from the measured decay of toluene, xylene, and other traditional precursors after the second spike for the two limiting cases, $\omega = 0$ and $\omega = 1$. These estimates were added to the log-linear fit and are indicated by the gray region in Figure 4a; the lower edge of the gray area corresponds to $\omega = 1$ and the upper edge to $\omega = 0$. The measured mass follows the bottom edge of the gray area, consistent with the suspended vapors remaining in equilibrium with the particles that have been lost to the walls.

Discussion

Photo-oxidation of diesel exhaust produces large amounts of SOA, greatly in excess of what can be explained by measured decay of traditional light aromatic gas-phase precursors. The large amounts of unexplained SOA observed in these laboratory experiments and by recent field studies (*6*, *8*, *27*) point to problems with existing atmospheric chemistry models and critical gaps in our laboratory data. Current SOA models are largely based on laboratory experiments that involve a single precursor or at most a simple mixture of precursors. The focus has been on high-volatility, high-flux species such as light aromatics, which dominate SOA production in existing models (*5*, *9*, *10*). These species have effective saturation concentrations between 10^7 and 10^9 μg m^{-3} and therefore produce SOA with low efficiency (typical yields are less than 10% at typical atmospheric conditions) (*9*). While tremendous progress has been made on constraining SOA yields of these species in simple systems, few experiments have considered SOA production under truly atmospherically relevant conditions. Our experiments investigate the SOA formation of actual emissions that include pre-existing aerosol and a complex mixture of gas-phase compounds at atmospherically relevant concentrations. Given this complexity, it is difficult to identify the source of the unexplained SOA, but our mixture is far more relevant to the atmosphere.

One concern is the applicability of current SOA models, which are based on data collected in much simpler experimental systems, to our chamber experiments. However, even if one doubles or triples the SOA from known precursors in the current models, the majority of the SOA remains unexplained. Therefore, the problem is not simply uncertainty in the SOA yields of existing precursors; there must be significant SOA production from unrecognized precursors.

We hypothesize that oxidation of low-volatility organic vapors explains the large amounts of unaccounted for SOA observed in these experiments (*25*). Diesel exhaust is a complex mixture of thousands of compounds that span a wide range of volatilities (*14*). A significant fraction of the emissions have effective saturation concentrations between 10^2 and 10^6 μg m^{-3} and therefore exist primarily in the gas phase at atmospheric conditions (and the conditions of our experiments) (*25*). Both gas−particle partitioning data (*25*) and analysis of quartz filter/polyurethane foam samples (*14*) indicate that the mass of these low-volatility vapors is several times that of the primary aerosol emissions. Oxidation of large saturated compounds produces acids, nitrates, and carbonyls, which have lower vapor pressures than the parent compounds (*28*). Given the low initial volatility of the parent compounds, we expect products to form SOA with a high efficiency. For example, SOA yields from *n*-alkanes increase dramatically with an increasing carbon number (*28*).

Little attention has been paid to the oxidation low-volatility organic vapors as a source of SOA. Current models do account for some SOA production from low-volatility vapors, such as large alkanes and cycloalkanes, but these vapors are predicted to contribute little SOA as compared to oxidation products of aromatics and biogenics (*5*, *9*, *10*). However, these vapors are poorly represented in VOC emissions inventories and chemical mechanisms, which are geared toward simulating tropospheric O_3. The measurement of low-volatility vapors currently requires using sorbents and chemical extraction and is thus uncommon. The limited available data from both source tests (*13*, *14*) and ambient measurements (*29*) indicates that the vast majority of the low-volatility organics, in both the gas and the particle phases, is an unresolved complex mixture of presumably branched and cyclic hydrocarbons. Therefore, the chemical identify of the majority of these vapors is not known. Finally, the SOA yields for low-volatility vapors used in current models are based on scientific judgment, not laboratory data (*30*, *31*).

Our results are based on experiments using a single-cylinder diesel engine whose emissions may not be representative of the much larger diesel engines used in the on- and off-road vehicles. Comparisons to literature data of the gas-phase organic data measured with PTR-MS and particle-phase organics data measured with AMS indicate that our emissions are at least qualitatively similar to other diesel engines (*14*, *32*). In addition, literature data indicate that larger diesel engines (*14*) and other combustion systems such as gasoline engines and fireplaces (*13*, *33*) emit substantial amounts of low-volatility organics that exist as vapors at atmospheric conditions. Therefore, we expect that photo-oxidation of exhaust from most combustion systems will form substantial amounts of SOA.

Acknowledgments

This research was supported by the EPA STAR program through the National Center for Environmental Research (NCER) under Grants RD-83108101 and R832162. This paper has not been subject to the EPA's required peer and policy review and therefore does not necessarily reflect the views of the Agency. No official endorsement should be inferred. PTR-MS and AMS were acquired with support from the NSF (ATM-0420842).

Supporting Information Available

Details on modeling SOA formation from traditional precursors. This material is available free of charge via the Internet at http://pubs.acs.org.

Literature Cited

(1) Kanakidou, M.; Seinfeld, J. H.; Pandis, S. N.; Barnes, I.; Dentener, F. J.; Facchini, M. C.; Van Dingenen, R.; Ervens, B.; Nenes, A.; Nielsen, C. J.; Swietlicki, E.; Putaud, J. P.; Balkanski, Y.; Fuzzi, S.; Horth, J.; Moortgat, G. K.; Winterhalter, R.; Myhre, C. E. L.; Tsigaridis, K.; Vignati, E.; Stephanou, E. G.; Wilson, J. Organic aerosol and global climate modeling: A review. *Atmos. Chem. Phys.* **2005**, *5*, 1053−1123.

(2) Turpin, B. J.; Saxena, P.; Andrews, E. Measuring and simulating particulate organics in the atmosphere: Problems and prospects. *Atmos. Environ.* **2000**, *34*, 2983−3013.

(3) Turpin, B. J.; Huntzicker, J. J. Identification of secondary organic aerosol episodes and quantitation of primary and secondary organic aerosol concentrations during SCAQS. *Atmos. Environ.* **1995**, *29*, 3527−3544.

(4) Cabada, J. C.; Pandis, S. N.; Subramanian, R.; Robinson, A. L.; Polidori, A.; Turpin, B. Estimating the secondary organic aerosol contribution to PM2.5 using the EC tracer method. *Aerosol Sci. Technol.* **2004**, *38*, 140−155.

(5) Pun, B. K.; Wu, S. Y.; Seigneur, C.; Seinfeld, J. H.; Griffin, R. J.; Pandis, S. N. Uncertainties in modeling secondary organic aerosols: Three-dimensional modeling studies in Nashville/western Tennessee. *Environ. Sci. Technol.* **2003**, *37*, 3647−3661.

(6) Volkamer, R.; Jimenez, J. L.; San Martini, F.; Dzepina, K.; Zhang, Q.; Salcedo, D.; Molina, L. T.; Worsnop, D. R.; Molina, M. J. Secondary organic aerosol formation from anthropogenic air pollution: Rapid and higher than expected. *Geophys. Res. Lett.* **2006**, *33*, L17811. doi:10.1029/2006GL026899.

(7) Zhang, Q.; Jimenez, J. L.; Canagaratna, M. R.; Allan, J. D.; Coe, H.; Ulbrich, I.; Alfarra, M. R.; Takami, A.; Middlebrook, A. M.; Sun, Y. L.; Dzepina, K.; Dunlea, E.; Docherty, K.; DeCarlo, P. F.; Salcedo, D.; Onasch, T.; Jayne, J. T.; Miyoshi, T.; Shimono, A.; Hatakeyama, S.; Takegawa, N.; Kondo, Y.; Schneider, J.; Drewnick, F.; Weimer, S.; Demerjian, K.; Williams, K.; Bower, K.; Bahreini, R.; Cotrell, L.; Griffin, R. J.; Rautiainen, J.; Sun, J. Y.; Zhang, Y. M.; Worsnop, D. R. Ubiquity and dominance of oxygenated species in organic aerosols in anthropogenically influenced Northern Hemisphere mid-latitudes. *Geophys. Res. Lett.* **2007**, *34*, L13801. doi:10.1029/2007GL029979.

(8) de Gouw, J. A.; Middlebrook, A. M.; Warneke, C.; Goldan, P. D.; Kuster, W. C.; Roberts, J. M.; Fehsenfeld, F. C.; Worsnop, D. R.; Canagaratna, M. R.; Pszenny, A. A. P.; Keene, W. C.; Marchewka, M.; Bertman, S. B.; Bates, T. S. Budget of organic carbon in a polluted atmosphere: Results from the New England Air Quality Study in 2002. *J. Geophys. Res., [Atmos.]* **2005**, *110*, D16305. doi:10.1029/2004JD005623.

(9) Koo, B. Y.; Ansari, A. S.; Pandis, S. N. Integrated approaches to modeling the organic and inorganic atmospheric aerosol components. *Atmos. Environ.* **2003**, *37*, 4757−4768.

(10) Vutukuru, S.; Griffin, R. J.; Dabdub, D. Simulation and analysis of secondary organic aerosol dynamics in the South Coast Air Basin of California. *J. Geophys. Res., [Atmos.]* **2006**, *111*, D10S12. doi:10.1029/2005JD006139.

(11) Odum, J. R.; Jungkamp, T. P. W.; Griffin, R. J.; Flagan, R. C.; Seinfeld, J. H. The atmospheric aerosol-forming potential of whole gasoline vapor. *Science* **1997**, *276*, 96−99.

(12) Odum, J. R.; Jungkamp, T. P. W.; Griffin, R. J.; Forstner, H. J. L.; Flagan, R. C.; Seinfeld, J. H. Aromatics, reformulated gasoline, and atmospheric organic aerosol formation. *Environ. Sci. Technol.* **1997**, *31*, 1890−1897.

(13) Schauer, J. J.; Kleeman, M. J.; Cass, G. R.; Simoneit, B. R. T. Measurement of emissions from air pollution sources. 5. C1−C32 organic compounds from gasoline-powered motor vehicles. *Environ. Sci. Technol.* **2002**, *36*, 1169−1180.

(14) Schauer, J. J.; Kleeman, M. J.; Cass, G. R.; Simoneit, B. R. T. Measurement of emissions from air pollution sources. 2. C1−C30 organic compounds from medium duty diesel trucks. *Environ. Sci. Technol.* **1999**, *33*, 1578−1587.

(15) Canagaratna, M. R.; Jayne, J. T.; Jimenez, J. L.; Allan, J. D.; Alfarra, M. R.; Zhang, Q.; Onasch, T. B.; Drewnick, F.; Coe, H.; Middlebrook, A.; Delia, A.; Williams, L. R.; Trimborn, A. M.; Northway, M. J.; DeCarlo, P. F.; Kolb, C. E.; Davidovits, P.; Worsnop, D. R. Chemical and microphysical characterization of ambient aerosols with the aerosol mass spectrometer. *Mass Spectrom. Rev.* **2007**, *26*, 185−222.

(16) Herndon, S. C.; Rogers, T.; Dunlea, E. J.; Jayne, J. T.; Miake-Lye, R.; Knighton, B. Hydrocarbon emissions from in-use commercial aircraft during airport operations. *Environ. Sci. Technol.* **2006**, *40*, 4406−4413.
(17) Atkinson, R.; Arey, J. Atmospheric degradation of volatile organic compounds. *Chem. Rev.* **2003**, *103*, 4605−4638.
(18) Grieshop, A. P.; Lipsky, E. M.; Pekney, N. J.; Takahama, S.; Robinson, A. L. Diesel and gasoline vehicle gaseous and fine particle emission factors measured in a highway tunnel in Pittsburgh, PA. *Atmos. Environ.* **2006**, *40* (Suppl. 2), 287−298.
(19) Pierce, J. R.; Weitkamp, E. A.; Sage, A. M.; Engelhart, G. J.; Robinson, A. L.; Donahue, N. M.; Adams, P. J. Estimating the contribution of wall loss and condensation/evaporation to aerosol size evolution in smog chamber experiments. *Aerosol Sci. Technol.* **2007**, in preparation.
(20) Sander, S. P.; Friedl, R. R.; Golden, D. M.; Kurylo, M. J.; Huie, R. E.; Orkin, V. L.; Moortgat, G. K.; Ravishankara, A. R.; Kolb, C. E.; Molina, M. J.; Finlayson-Pitts, B. J. *Chemical Kinetics and Photochemical Data for Use in Atmospheric Studies, Evaluation Number 14*; JPL Publication 02-25; Jet Propulsion Laboratory: Pasadena, CA, 2003.
(21) Atkinson, R. Kinetics and mechanisms of the gas-phase reactions of the hydroxyl radical with organic compounds under atmospheric conditions. *Chem. Rev.* **1986**, *86*, 69−201.
(22) Seinfeld, J. H.; Pandis, S. N. *Atmospheric Chemistry and Physics: From Air Pollution to Climate Change*; John Wiley and Sons, Inc.: New York, 1998.
(23) Molina, M. J.; Ivanov, A. V.; Trakhtenberg, S.; Molina, L. T. Atmospheric evolution of organic aerosol. *Geophys. Res. Lett.* **2004**, *31*, L22104. doi:10.1029/2004GL020910.
(24) Lipsky, E. M.; Robinson, A. L. Effects of dilution on fine particle mass and partitioning of semivolatile organics in diesel exhaust and wood smoke. *Environ. Sci. Technol.* **2006**, *40*, 155−162.
(25) Robinson, A. L.; Donahue, N. M.; Shrivastava, M. K.; Weitkamp, E. A.; Sage, A. M.; Grieshop, A. P.; Lane, T. E.; Pandis, S. N.; Pierce, J. R. Rethinking organic aerosols: Semivolatile emissions and photochemical aging. *Science* **2007**, *315*, 1259−1262.
(26) Sage, A. M.; Weitkamp, E. A.; Robinson, A. L.; Donahue, N. M. Evolving mass spectra of the oxidized component of organic aerosol: Results from aerosol mass spectrometer analyses of aged diesel emissions. *Atmos. Chem. Phys. Discuss.* **2007**, *7*, 10065−10096.
(27) Zhang, Q.; Worsnop, D. R.; Canagaratna, M. R.; Jimenez, J. L. Hydrocarbon-like and oxygenated organic aerosols in Pittsburgh: Insights into sources and processes of organic aerosols. *Atmos. Chem. Phys.* **2005**, *5*, 3289−3311.
(28) Lim, Y. B.; Ziemann, P. J. Products and mechanism of secondary organic aerosol formation from reactions of *n*-alkanes with OH radicals in the presence of NO_x. *Environ. Sci. Technol.* **2005**, *39*, 9229−9236.
(29) Fraser, M. P.; Cass, G. R.; Simoneit, B. R. T.; Rasmussen, R. A. Air quality model evaluation data for organics. 4. C2−C36 nonaromatic hydrocarbons. *Environ. Sci. Technol.* **1997**, *31*, 2356−2367.
(30) Pandis, S. N.; Harley, R. A.; Cass, G. R.; Seinfeld, J. H. Secondary organic aerosol formation and transport. *Atmos. Environ.* **1992**, *26*, 2269−2282.
(31) Grosjean, D.; Seinfeld, J. H. Parameterization of the formation potential of secondary organic aerosols. *Atmos. Environ.* **1989**, *23*, 1733−1747.
(32) Canagaratna, M. R.; Jayne, J. T.; Ghertner, D. A.; Herndon, S.; Shi, Q.; Jimenez, J. L.; Silva, P. J.; Williams, P.; Lanni, T.; Drewnick, F.; Demerjian, K. L.; Kolb, C. E.; Worsnop, D. R. Chase studies of particulate emissions from in use New York City vehicles. *Aerosol Sci. Technol.* **2004**, *38*, 555−573.
(33) Schauer, J. J.; Kleeman, M. J.; Cass, G. R.; Simoneit, B. R. T. Measurement of emissions from air pollution sources. 3. C1−C29 organic compounds from fireplace combustion of wood. *Environ. Sci. Technol.* **2001**, *35*, 1716−1728.
(34) Tobias, H. J.; Beving, D. E.; Ziemann, P. J.; Sakurai, H.; Zuk, M.; McMurry, P. H.; Zarling, D.; Waytulonis, R.; Kittelson, D. B. Chemical analysis of diesel engine nanoparticles using a nano-DMA/thermal desorption particle beam mass spectrometer. *Environ. Sci. Technol.* **2001**, *35*, 2233−2243.

Received for review January 24, 2007. Revised manuscript received May 29, 2007. Accepted July 27, 2007.

ES070193R